Technical Reference on Hydrogen Compatibility of Materials

Nickel Alloys:
Solid-Solution Alloys
Ni-Cr Alloys (code 5110)

Prepared by:

C. San Marchi, Sandia National Laboratories, Livermore CA

Editors
C. San Marchi
B.P. Somerday
Sandia National Laboratories

This report may be updated and revised periodically in response to the needs of the technical community; up-to-date versions can be requested from the editors at the address given below or downloaded at http://www.sandia.gov/matlsTechRef/. The content of this report will also be incorporated into a Sandia National Laboratory report (SAND2008-1163); the most recent version can be obtained from the link above. The success of this reference depends upon feedback from the technical community; please forward your comments, suggestions, criticisms and relevant public-domain data to:

Sandia National Laboratories
Matls Tech Ref
C. San Marchi (MS-9402)
7011 East Ave
Livermore CA 94550.

Sandia National Laboratories is a multi-program laboratory operated by Sandia Corporation, a wholly owned subsidiary of Lockheed Martin Corporation, for the U.S. Department of Energy's National Nuclear Security Administration under contract DE-AC04-94AL85000.

Technical Reference on Hydrogen Compatibility of Materials

Nickel Alloys:

Solid-Solution Ni-Cr Alloys (code 5110)

1. General

Solid-solution Ni-Cr alloys are used in specialty applications for their combination of strength and high-corrosion resistance, especially at elevated temperature. For the purposes of this discussion, all non-precipitation-hardening, nickel-base alloys with chromium greater than about 10 wt% are considered to be solid-solution Ni-Cr alloys. This represents a wide range of alloy compositions, which makes it difficult to generalize the effects of materials variables on hydrogen-assisted fracture. On the other hand, given the relatively limited data available to assess the effects of gaseous hydrogen on these alloys, this is a convenient classification. The nominally single-phase microstructure of the solid-solution Ni-Cr alloys also suggests a single classification for the purposes of discussing the effects of hydrogen on material properties.

The solid-solution Ni-Cr alloys have similar (single-phase) microstructure as the austenitic stainless steels, which provides an analogy for understanding hydrogen interactions, since the latter have been more extensively studied in gaseous hydrogen environments. A number of studies have drawn this parallel, hypothesizing that hydrogen enhances localization of deformation in solid-solution Ni-Cr alloys and that the relative resistance to hydrogen-assisted fracture can be related to the intrinsic character of deformation in the materials [1, 2]. Alloys with greater stacking fault energy show better resistance to hydrogen-assisted fracture in tensile tests; for example, relatively low-chromium content in the solid-solution Ni-Cr-Fe alloys increases stacking fault energy (for constant iron content) and resistance to hydrogen-assisted fracture [1], while in austenitic stainless steels high-nickel content increases stacking fault energy and resistance to hydrogen-assisted fracture [3, 4]. Carbide precipitation, especially on grain boundaries, similarly enhances hydrogen-assisted fracture in solid-solution Ni-Cr alloys [2, 5] as in austenitic stainless steels [6, 7]. There are also important differences between solid-solution Ni-Cr alloys and austenitic stainless steels. Although generally absent from the austenitic stainless steels (with the possible exception of high-nitrogen stainless steel alloys), short-range ordering is an important phenomenon in Ni-Cr alloys that enhances hydrogen-assisted fracture [8-12]. Impurity segregation to grain boundaries (particularly phosphorus) is also implicated in hydrogen-assisted fracture of solid-solution Ni-Cr alloys [10-13] to a greater extent than in austenitic stainless steels.

Environmental variables also are expected to have similar effects on hydrogen-assisted fracture in both solid-solution Ni-Cr alloys and the austenitic stainless steels. For example, low temperature enhances localized deformation and exacerbates hydrogen-assisted fracture.

In summary, materials characteristics (such as ordering and low stacking fault energy) as well as environmental variables (such as temperature) that promote slip localization in solid-solution Ni-Cr alloys promote hydrogen-assisted fracture. In addition, carbide precipitation and grain boundary segregation also exacerbate hydrogen-assisted fracture, since their influence is enhanced by the role of hydrogen in localizing deformation [2].

1.1 Composition and microstructure

The solid-solution Ni-Cr alloys are highly alloyed, typically containing chromium in the range of 15 to 30 wt% (depending on the specifics of the alloy). These alloys generally contain 2 to 20 wt% iron, as well as significant amounts of molybdenum and cobalt in some alloys (as much as 18 and 15 wt% respectively). Tungsten and niobium are also present in modest amounts in some alloy variations. The elements that promote γ' precipitation (aluminum and titanium in particular) are generally limited to significantly less than 1 wt% each. Table 1.1.1 lists compositional ranges for several common solid-solution Ni-Cr alloys.

The solid-solution Ni-Cr alloys are nominally single phase with the FCC crystal structure, which endows them with characteristics similar to the austenitic stainless steels. Carbon contents are generally low, although the alloys can still be susceptible to precipitation of carbides at elevated temperature, particularly on grain boundaries. In addition, Ni-Cr alloys can be susceptible to ordering, which impacts deformation and the transport of hydrogen.

1.2 Common designations

Tradenames are commonly used for these alloys, including Inconel, Hastelloy, Nimonic, and many others. These same tradenames are also applied to precipitation-strengthened alloys. The tradename is occasionally dropped, such as alloy 600 and Alloy 22 in reference to Inconel 600 and Hastelloy C-22, respectively. For the purposes of this document, the Incoloy alloys (e.g., Incoloy 800 and 900 alloys) are considered iron alloys and included in the appropriate chapters.

2. Permeability, Diffusivity and Solubility

There are a number of gas-permeation studies that report the transport properties of hydrogen in the nickel-base alloys. The permeation, diffusion and solubility parameters from these studies are given in Table 2.1. The magnitude and temperature dependence of the hydrogen transport parameters are similar to those reported for austenitic stainless steels (Figures 2.1, 2.2 and 2.3). In addition, thermal precharging with hydrogen to equilibrium saturation can be used to determine the solubility at a specific temperature (provided that the precharging temperature is sufficiently high that hydrogen is not trapped and that hydrogen diffusivity is sufficiently low to prevent hydrogen loss after precharging). Figure 2.2 summarizes the solubility that is calculated from studies reporting the hydrogen content of specimens that were saturated in gaseous hydrogen at elevated temperature.

The magnitude and temperature dependence of hydrogen permeability is very consistent between studies on various solid-solution Ni-Cr alloys and values reported for austenitic stainless steels (Figure 2.1). The diffusivity of hydrogen in the solid-solution Ni-Cr alloys appears to be slightly greater than for austenitic stainless steels. Diffusion studies using isothermal desorption [14] and electrochemical [15] methods give relationships that are consistent with the higher temperature, gas-permeation measurements. In addition, these diffusion studies suggest that diffusivity depends on composition of the Ni-Cr alloys: for example, diffusivity of hydrogen in Inconel 600 is greater than in Inconel 690 by a factor of about five [14, 15]. Alloys with high chromium content (such as Inconel 690) have greater solubility for hydrogen than alloys with comparatively lower chromium content (such as Inconel 600); this is shown in Figure 2.4. Thus, alloys with comparatively high chromium content have relatively low hydrogen diffusivity (since the permeability is nominally constant and the transport properties are related: $\Phi = DS$). The

calculated values of solubility given in Table 2.2 are also shown on the plot of solubility in Figure 2.3, further demonstrating the range of solubility that can be expected for solid-solution Ni-Cr alloys with different composition. Other alloying elements may also have a significant impact, particularly those that can vary over a wide range such as iron, molybdenum, and cobalt, but their effect on transport properties has not been studied.

Strain-hardening appears to have essentially no effect on the apparent diffusivity for some alloys (such as, Inconel 690 [14, 15] and Hastelloy C-276 [16, 17]), but can have modest effects on the apparent diffusivity in other alloys (such as, Inconel 600 [14, 15] and Hastelloy G [17]). Ordering has been invoked to explain small reductions of hydrogen diffusivity in Hastelloy C-276 subjected to low-temperature aging (473K to 773K) [16], although no reduction of hydrogen diffusivity is observed for Hastelloy G subjected to the same aging treatments [17]. In general, however, the role of strain-hardening and ordering on hydrogen transport in solid-solution Ni-Cr alloys is not well understood.

Hydrogen trapping in solid-solution Ni-Cr alloys is generally attributed to carbides [14, 17], as well as dislocations [15]. In alloys with very low carbon content (such as Hastelloy C-276), hydrogen trapping is reported to be absent [16, 17] or attributed to phosphorus segregation to grain boundaries [18].

3. Mechanical Properties: Effects of Gaseous Hydrogen

3.1 Tensile properties

3.1.1 Smooth tensile properties

The effects of hydrogen on the tensile properties of solid-solution Ni-Cr alloys can be significant. In general, the tensile ductility is reduced when these alloys are tested in high-pressure gaseous hydrogen [7, 19], with the exception of Hastelloy X, which shows no effects of gaseous hydrogen at room temperature [20]. The magnitude of the reported reduction in tensile ductility can vary significantly: Hastelloy C-22 displays grain boundary fracture and relatively low tensile ductility in gaseous hydrogen at pressure of 70 MPa [7, 19], while Inconel 600 displays transgranular fracture and significantly greater tensile ductility in gaseous hydrogen at pressure of 70 MPa [7]. While the absolute values of the tensile properties are not reported in these studies, the properties of Inconel 625 and Hastelloy X in gaseous hydrogen at 34.5 MPa are reported, Table 3.1.1.1. Tensile tests have also been performed on Hastelloy X at elevated temperature in gaseous hydrogen (34.5 MPa), and for Inconel 625 at both cryogenic and elevated temperature in gaseous hydrogen, Table 3.1.1.2. The effects of hydrogen on Inconel 625 are significantly reduced at both temperature extremes.

Testing of hydrogen-precharged materials [1, 21-23] also shows reduction of tensile ductility. Inconel 600 appears to display less reduction of ductility when hydrogen precharged than other solid-solution Ni-Cr alloys, Table 3.1.1.1. In a separate study, Hastelloy X shows significantly less reduction of tensile elongation than Inconel 600 [5]. Fracture surfaces tend to be rather complicated with the most affected alloys showing evidence of intergranular fracture and strong slip localization [1, 2, 23].

The range of tensile ductility that is observed for solid-solution Ni-Cr alloys in the presence of hydrogen is generally attributed to microstructural characteristics that affect deformation.

Symons, for example, studied the effect of Cr content on laboratory heats similar to Inconel 600 (Ni-15Cr-8Fe) and Inconel 690 (Ni-30Cr-8Fe) [1], showing that chromium content is an important materials variable (all else being equal), Table 3.1.1.3. Symons related chromium content to the stacking fault energy: alloys with greater resistance to hydrogen-assisted fracture have higher stacking fault energy, which correlates with lower chromium content in the alloys studied by Symons [1]. This is analogous to the role attributed to nickel in austenitic stainless steels [24] (although stacking fault energy increases as nickel increases), as well as nitrogen in 21Cr-6Ni-9Mn austenitic stainless steel [25]. Other microstructural influences that reduce tensile ductility include carbide precipitation [5, 22], impurity segregation [13] and ordering [8, 9, 11], all of which can generally be a concern for solid-solution Ni-Cr alloys.

The effects of temperature and strain rate were explored by Chene and Brass for Inconel 600 using cathodic precharging in molten salts to about 35 wppm hydrogen and testing in air (uniform saturation of hydrogen in 5 mm thick flat tensile specimens) [26]. They found the elongation to show a minimum at temperature near 240K for hydrogen-precharged specimens and no effect of temperature on elongation in the absence of hydrogen in the temperature range from 240K to 470K. At very low temperature (77K), there was essentially no change in elongation due to hydrogen. At temperature of 513K, the elongation was also unchanged by hydrogen although significant hydrogen desorbed from the specimen during testing. In addition, Chene and Brass observed little effect of strain rate near room temperature for strain rates less than about 10^{-3} s^{-1}, in contrast to another study where the tensile elongation due to thermally precharged hydrogen was found to be decrease with strain rate to lower strain rates [5].

3.1.2 Notched tensile properties

Strength and ductility (RA) of notched tensile specimens of Inconel 625 are reduced in gaseous hydrogen compared to gaseous helium, Table 3.1.2.1. The reduction of ductility is significantly greater than the reduction of notched tensile strength. Hastelloy X displays about a 10% reduction of notched strength and ductility in gaseous hydrogen, in contrast to the smooth tensile tests where no effects of hydrogen are observed for the same testing conditions. At elevated temperature (951 K), gaseous hydrogen at pressure of 34.5 MPa has no effect on tensile properties of Inconel 625 and Hastelloy X, Table 3.1.2.2. Also at cryogenic temperature (144 K) in gaseous hydrogen at pressure of 34.5 MPa, the RA of Inconel 625 is only modestly affected (Table 3.1.2.2) compared to the reduction observed at room temperature (Table 3.1.2.1).

Tensile elongation was found to depend on the stress concentration factor in hydrogen-precharged Inconel 600 and Hastelloy X [5]. The relative decrease of tensile elongation for notched Inconel 600 ($K_t = 5.5$) was found to approximately double relative to smooth tensile specimens. For Hastelloy X, tensile elongation was relatively unaffected by hydrogen for smooth tensile specimens, compared to approximately 25% reduction in tensile elongation with a notch ($K_t = 5.5$).

3.2 Fracture mechanics

The fracture toughness of Inconel 690 is significantly reduced when the material is hydrogen precharged, Table 3.2.1 [22], while the fracture toughness of Inconel 625 in gaseous hydrogen is essentially unchanged compared to tests in gaseous helium [20, 27, 28]. The relative fracture toughness of the two alloys, however, is substantially different: the fracture toughness of the Inconel 690 is almost five times greater than the fracture toughness of Inconel 625. These

differences may reflect the difference in strength of the tested alloys (the Inconel 625 was not fully annealed), or may reflect 30 years of improvements in materials processing (the study on Inconel 625 was performed in the early 1970s, while the study on Inconel 690 is from the late 1990s). The fracture toughness of currently available and properly annealed Inconel 625 is likely consistent with the values reported here for Inconel 690. In any case, the hydrogen-affected fracture toughness of Inconel 690 remains relatively large compared to values of fracture toughness from Refs. [20, 27, 28] on Inconel 625 in an inert environment and other structural metals, such as aluminum alloys. The fracture toughness at cryogenic temperature (144 K) is greater than at room temperature and unaffected by gaseous hydrogen, Table 3.2.2.

Carbide precipitation at grain boundaries (i.e., sensitization due to thermal exposure) does not impact the fracture toughness of Inconel 690 in air, but reduces the fracture toughness in the hydrogen-precharged condition by a factor of more than 2, compared to non-sensitized material [22].

3.3 Fatigue

Low-cycle fatigue of Inconel 625 and Hastelloy X in gaseous hydrogen at pressure of 34.5 MPa is reported in several reports for NASA [20, 27]. The data is reproduced in Figure 3.3.1, showing a significant reduction in number of cycles to failure for a given value of total strain. This reduction is greater for Inconel 625 than for Hastelloy X, which is consistent with results from tensile testing.

3.4 Creep

A limited set of creep rupture data are available for Inconel 625 in Refs [20, 27] at temperature of 951 K. Rupture occurred in less than 50 hours at stress of 286 MPa in gaseous hydrogen at pressure of 34.5 MPa. Specimens in gaseous hydrogen failed during loading at stresses as low as 310 MPa. In comparison, rupture took greater than 20 hours for substantially higher stresses (430 MPa) in gaseous helium. In short, gaseous hydrogen significantly enhances creep in Inconel 625.

3.5 Impact

No known published data in gaseous hydrogen.

3.6 Disk rupture testing

Disk rupture tests show that nickel-base alloys are extremely sensitive to hydrogen-assisted fracture in gaseous environments [29].

4. Fabrication

4.1 Primary processing

Impurity segregation, as well as alloy segregation, is important issues during the production of nickel alloys. One study suggests that impurity segregation at grain boundaries in Inconel 600 enhances resistance to hydrogen-assisted fracture [13], while most studies implicate impurity segregation in exacerbating hydrogen-assisted fracture. Macrosegregation may promote

hydrogen-assisted fracture in Ni-Cr alloys in the same way that macrosegregation enhances hydrogen-assisted fracture in austenitic stainless steels [30].

4.2 Heat treatment

Proper heat treating and appropriate thermal exposure is an important consideration for some solid-solution Ni-Cr alloys, due to ordering and sensitization (carbide precipitation at grain boundaries). The effects of ordering and sensitization may not be apparent at ambient conditions, but when combined with hydrogen these effects can be substantial [22].

4.3 Properties of welds

Alloys with niobium or titanium additions (such as Inconel 625) are designed to control sensitization during welding as in type 321 and 347 austenitic stainless steels. The smooth tensile properties (Table 4.3.1), notched tensile properties (Table 4.3.2) and fracture toughness (Table 4.3.3) of the fusion zone in welded Inconel 625 are reported in Ref. [20]. Gaseous hydrogen had significantly less effect on the properties of the welds compared to the base metal, likely due to the lower strength of the fusion zone of the weld compared to the base metal.

5. References

1. DM Symons. Hydrogen Embrittlement of Ni-Cr-Fe Alloys. Metall Mater Trans 28A (1997) 655-663.
2. DM Symons. The Effect of Carbide Precipitation on the Hydrogen-Enhanced Frature Behavior of Alloy 690. Metall Mater Trans 29A (1998) 1265-1277.
3. GR Caskey. Hydrogen Compatibility Handbook for Stainless Steels (DP-1643). EI du Pont Nemours, Savannah River Laboratory, Aiken SC (June 1983).
4. GR Caskey. Hydrogen Effects in Stainless Steels. in: RA Oriani, JP Hirth and M Smialowski, editors. Hydrogen Degradation of Ferrous Alloys. Park Ridge NJ: Noyes Publications (1985) p. 822-862.
5. M Hasegawa and M Osawa. Hydrogen damage of nickel-base heat resistant alloys. Transactions ISIJ 21 (1981) 25-31.
6. G Han, J He, S Fukuyama and K Yokogawa. Effect of strain-induced martensite on hydrogen environment embrittlement of sensitized austenitic stainless steels at low temperatures. Acta Mater 46 (1998) 4559-4570.
7. S Fukuyama, M Imade and K Yokogawa. Development of new material testing appartus in high-pressure hydrogen and evaluation of hydrogen gas embrittlement of metals (PVP2007-26820). in: Proceedings of PVP-2007: ASME Pressure Vessels and Piping Division Conference, 2007, San Antonion TX. ASME (July 22-26, 2007)
8. K Miyata and M Igarashi. Effect of ordering in susceptibility to hydrogen embrittlement of a Ni-base superalloy. Metall Trans 23A (1992) 953-961.
9. RJ Coyle, JA Kargol and NF Fiore. Hydrogen-assisted ductile fracture in a Ni-base superalloy. Scr Metall 14 (1980) 939-942.
10. N Sridhar, JA Kargol and NF Fiore. Effect of low temperature aging on hydrogen-induced crack growth in a Ni-base superalloy. Scr Metall 14 (1980) 1257-1260.
11. RJ Coyle, JA Kargol and NF Fiore. The effect of aging on hydrogen embrittlement of a nickel alloy. Metall Trans 12A (1981) 653-658.

12. JA Kargol and B Ladna. The roles of ordering and impurity segregation on the hydrogen assisted crack propagation in nickel base stainless alloys. Scr Metall 16 (1982) 191-195.
13. M Cornet, C Bertrand and M Da Cunha Belo. Hydrogen embrittlement of ultrapure alloys of the Inconel 600 type: influence of the additions of elements (C, P, Sn, Sb). Metall Trans 13A (1982) 141-144.
14. DM Symons, GA Young and JR Scully. The effect of strain on the trapping of hydrogen at grain-boundary carbides in Ni-Cr-Fe alloys. Metall Mater Trans 32A (2001) 369-377.
15. M Uhlemann and BG Pound. Diffusivity, solubility and trapping behavior of hydrogen in alloys 600, 690tt and 800. Corros Sci 40 (1998) 645-662.
16. DA Mezzanotte, JA Kargol and NF Fiore. Hydrogen transport in a Ni-base superalloy. Scr Metall 14 (1980) 219-223.
17. DA Mezzanotte, JA Kargol and NF Fiore. Hydrogen transport in nickel base stainless alloys. Metall Trans 13A (1982) 1181-1186.
18. BG Pound. Hydrogen trapping in work-hardened alloys. Acta Metall Mater 39 (1991) 2099-2105.
19. S Fukuyama, M Imade, T Iijima and K Yokogawa. Development of new material testing apparatus in 230 MPa hydrogen and evaluation of hydrogen gas embrittlement of metals. in: Proceedings of PVP-2008: ASME Pressure Vessels and Piping Division Conference, 2008, Chicago IL. ASME (July 27-31, 2008)
20. JA Harris and MCV Wanderham. Properties of Materials in High Pressure Hydrogen at Cryogenic, Room, and Elevated Temperatures. Pratt and Whitney Aircraft (report no. FR-5768) for the National Aeronautics and Space Administration (Marshall Space Flight Center), West Palm Beach FL (Jul 1973).
21. AW Thompson. Hydrogen-assisted fracture in single-phase nickel alloys. Scr Metall 16 (1982) 1189-1192.
22. DM Symons. The effect of carbide precipitation on the hydrogen-enhanced fracture behavior of alloy 690. Metall Mater Trans 29A (1998) 1265-1277.
23. C San Marchi, T Zaleski, S Lee, NYC Yang and B Stuart. Effect of laser peening on the hydrogen compatibility of corrosion-resistant nickel alloy. Scr Mater 58 (2008) 782-785.
24. BC Odegard, JA Brooks and AJ West. The Effect of Hydrogen on Mechanical Behavior of Nitrogen-Strengthened Stainless Steel. in: AW Thompson and IM Bernstein, editors. Effect of Hydrogen on Behavior of Materials. Proceedings of an International Conference on Effect of Hydrogen on Behavior of Materials (Moran WY, 1975), volume New York: The Metallurgical Society of AIME (1976) p. 116-125.
25. RE Stoltz and JB VanderSande. The Effect of Nitrogen on Stacking Fault Energy of Fe-Ni-Cr-Mn Steels. Metall Trans 11A (1980) 1033-1037.
26. J Chene and AM Brass. Role of temperature and strain rate on the hydrogen-induced intergranular rupture in alloy 600. Metall Mater Trans 35A (2004) 457-464.
27. JA Harris and MCV Wanderham. Propeties of Materials in High Pressure Hydrogen at Cryogenic, Room, and Elevated Temperatures (Annual Report). Pratt and Whitney Aircraft (report no. FR-4566) for the National Aeronautics and Space Administration (Marshall Space Flight Center), West Palm Beach FL (1971).
28. RJ Walter and WT Chandler. Influence of Gaseous Hydrogen on Metals: Final Report. Rocketdyne for the National Aeronautics and Space Administration, Canoga Park CA (Oct 1973).

29. J-P Fidelle. Present status of the disk pressure test for hydrogen embrittlement. in: L Raymond, editor. Test Methods for Hydrogen Embrittlement: Prevention and Control, ASTM STP 962, American Society for Testing and Materials. (1988) p. 153-172.
30. T Michler, Y Lee, RP Gangloff and J Naumann. Influence of macro segregation on hydrogen environment embrittlement of SUS 316L stainless steel. Int J Hydrogen Energy 34 (2009) 3201-3209.
31. ASTM. ASTM DS-56H, Metals and Alloys in the UNIFIED NUMBERING SYSTEM (SAE HS-1086 OCT01). 2001.
32. T Tanabe, Y Tamanishi, K Sawada and S Imoto. Hydrogen Transport in Stainless Steels. J Nucl Mater 122&123 (1984) 1568-1572.
33. N Kishimoto, T Tanabe, T Suzuki and H Yoshida. Hydrogen diffusion and solution at high temperatures in 316L stainless steel and nickel-base heat-resistant alloys. J Nucl Mater 127 (1985) 1-9.
34. AS Schmidt, F Verfuss and E Wicke. Studies on the permeation of hydrogen and tritium through heat resistant alloys. J Nucl Mater 131 (1985) 247-260.
35. E Rota, F Waelbroeck, P Weinhold and J Winter. Measurements of surface and bulk properties for the interaction of hydrogen with Inconel 600. J Nucl Mater 111 & 112 (1982) 233-239.
36. C San Marchi, BP Somerday and SL Robinson. Permeability, Solubility and Diffusivity of Hydrogen Isotopes in Stainless Steels at High Gas Pressure. Int J Hydrogen Energy 32 (2007) 100-116.

Table 1.1.1. Compositions (wt%) of common commercial solid-solution Ni-Cr alloys [31].

UNS No	Common Name	Ni	Cr	Fe	Mo	Co	W	Al	Ti	Mn	Si	C	other
N06002	Hastelloy X (Ni–22Cr–18Fe–8Mo)	Bal	20.5 23.0	17.0 20.0	8.0 10.0	0.5 2.5	0.20 1.0	—	—	1.00 max	1.00 max	0.05 0.15	0.040 max P; 0.030 max S
N06007	Hastelloy G (Ni–23Cr–19Fe–6Mo)	Bal	21.0 23.5	18.0 21.0	5.5 7.5	2.5 max	1.0 max	—	—	1.0 2.0	1.0 max	0.05 max	1.75-2.5 Nb; 1.5-2.5 Cu; 0.04 max P; 0.03 max S
N06022	Hastelloy C-22 (Ni–22Cr–3Fe–13Mo)	Bal	20.0 22.5	2.0 6.0	12.5 14.5	2.5 max	2.5 3.5	—	—	0.50 max	0.08 max	0.015 max	0.35 max V; 0.02 max P; 0.02 max S
N06075	Nimonic 75 (Ni–20Cr–4Fe)	Bal	18.0 21.0	5.00 max	—	—	—	—	0.20 0.60	1.00 max	1.00 max	0.08 0.15	0.50 max Cu
N06600	Inconel 600 (Ni–15Cr–8Fe)	Bal (72 min)	14.00 17.00	6.00 10.00	—	—	—	—	—	1.00 max	0.50 max	0.15 Max	0.50 max Cu; 0.040 max P; 0.015 max S
N06617	Inconel 617 (Ni–22Cr–9Mo–12Co)	Bal (44.5 min)	20.0 24.0	3.00 max	8.0 10.0	10.0 15.0	—	0.80 1.50	0.60 max	1.00 max	1.00 max	0.05 0.15	0.50 max Cu; 0.006 max B; 0.015 max S;
N06625	Inconel 625 (Ni–22Cr–9Mo–4Nb)	Bal	20.0 23.0	5.0 max	8.0 10.0	—	—	0.40 max	0.40 max	0.50 max	0.50 max	0.10 max	3.15-4.15 Nb; 0.015 max P; 0.015 max S
N06690	Inconel 690 (Ni–29Cr–9Fe)	Bal (58 min)	27.0 31.0	7.0 11.0	—	—	—	0.50 max	—	0.50 max	0.50 max	0.05 max	0.50 max Cu; 0.015 max S
N10276	Hastelloy C-276 (Ni–16Cr–5Fe –16Mo)	Bal	14.5 16.5	4.0 7.0	15.0 17.0	2.5 max	3.0 4.5	—	—	1.0 max	0.08 max	0.02 max	0.35 max V; 0.030 max P; 0.030 max S

Table 1.1.2. Compositions (wt%) of solid-solution Ni-Cr alloys used in studies with hydrogen.

Heat	alloy	Ni	Cr	Fe	Mo	Co	W	Al	Ti	Mn	Si	C	other	Ref.
H73a	Inconel 625 Partially annealed bar (dia. 19 mm)	Bal	21.6	2.14	9.10	0.05	—	0.17	0.06	0.01	0.08	0.052	3.82 Nb; 0.005 P; 0.005 S	[20]
H73b	Inconel 625 Partially annealed bar (dia. 108 mm)	Bal	21.82	1.79	9.05	—	—	0.18	0.20	0.02	0.10	0.04	3.92 Nb; 0.004 P; 0.005 S	[20]
H73c	Hastelloy X Solutionized bar (dia. 19 mm)	Bal	22.31	18.36	8.27	1.60	0.51	—	—	0.61	0.71	0.074	0.0014 B; 0.016 P; 0.006 S	[20]
W73	Inconel 625 Partially annealed bar (32x70 mm)	Bal	21.14	2.55	8.97	0.07	—	0.20	0.11	0.05	0.20	0.047	3.73 Nb; 0.008 P; 0.003 S	[28]
T84a	Inconel 600	(72)	(16)	(8)	—	—	—	—	—	—	—	—	—	[32]
T84b	Nichrome	(77)	(20)	(2)	—	—	—	—	—	—	—	—	—	[32]
K85a	Inconel 600	Bal	15.9	7.0	—	—	—	0.32	0.41	0.45	0.25	0.047	0.20 Cu	[33]
K85b	Hastelloy X	Bal	20.7	19.7	8.9	1.6	0.48	—	—	0.15	0.14	0.10	0.01 Cu	[33]
S85	Nimonic PE 13	Bal	21.0	19.1	8.8	1.6	0.65	—	0.04	0.37	0.44	0.054	0.07 Cu	[34]
S98a	Inconel 690	Bal	27.5	8.1	—	0.26	—	0.26	0.25	—	0.1	0.02	0.004 B; 0.006 P; 0.001 S	[22]
S98b	Inconel 690	Bal	28.3	8.4	—	0.35	—	—	—	—	0.3	0.03	0.004 B 0.013 P; 0.001 S;	[22]
S08	Hastelloy C-22	Bal	21.8	3.8	13.0	—	3.0	—	—	0.34	0.08	0.002	—	[23]

Table 2.1. Permeability, diffusivity and solubility relationships for solid-solution Ni-Cr alloys. These relationships are plotted in Figures 2.1, 2.2 and 2.3 for permeability, diffusivity and solubility respectively.

Material	Temperature Range (K)	Pressure Range (MPa)	$\Phi = \Phi_o \exp(-E_\Phi / RT)$		$D = D_o \exp(-E_D / RT)$		$S = S_o \exp(-E_S / RT)$		Ref.
			Φ_o $\left(\frac{\text{mol H}_2}{\text{m} \cdot \text{s} \cdot \text{MPa}^{1/2}}\right)$	E_Φ $\left(\frac{\text{kJ}}{\text{mol}}\right)$	D_o $\left(\frac{\text{m}^2}{\text{s}}\right)$	E_D $\left(\frac{\text{kJ}}{\text{mol}}\right)$	S_o $\left(\frac{\text{mol H}_2}{\text{m}^3 \cdot \text{MPa}^{1/2}}\right)$	E_S $\left(\frac{\text{kJ}}{\text{mol}}\right)$	
Inconel 600	423–673	—	19.9×10^{-6}	55.2	1.70×10^{-6}	49.8	11.7	5.4	[35]
Inconel 600 (heat K85a)	873–1173	0.1–0.7	783×10^{-6}	63.7	0.49×10^{-6}	42.5	1600	21.2	[33]
Inconel 600 (heat T84a)	500–1200	0.001 –0.1	950×10^{-6}	66.2	0.136×10^{-6}	37.7	6990	28.5	[32]
Hastelloy X (heat K85b)	873–1173	0.1–0.7	881×10^{-6}	64.6	0.490×10^{-6}	43.4	1800	21.2	[33]
Nichrome (heat T84b)	500–1200	0.001 –0.1	220×10^{-6}	60.3	0.111×10^{-6}	37.2	1980	23.1	[32]
Nimonic PE13 (heat S85)	500–1200	0.001 –0.01	36.2×10^{-6}	52.3	0.092×10^{-6}	33.8	394	18.5	[34]
Austenitic stainless steels	—	—	120×10^{-6}	59.8	0.89×10^{-6}	53.9	135	5.9	[36]

Table 2.2. Solubility of hydrogen in several solid-solution Ni-Cr alloys, determined after thermal precharging in gaseous hydrogen at elevated temperature and pressure.

Material	Precharging temperature (K)	Precharging pressure (MPa)	Reported hydrogen concentration (wppm)	Solubility † $\left(\frac{\text{mol } H_2}{m^3 \cdot MPa^{1/2}}\right)$	Cr content (wt%)	Ref.
Inconel 600	723	30	40 cm^3/100g	25.7	15.4	[5]
Inconel 690 (heat S98a)	558	13	38	41.9	27.5	[22]
		34	59.5	39.1		
Inconel 690 (heat S98b)		13	38.5	42.5	28.3	
		34	60	39.5		
Ni-6Cr-8Fe	558	13	25	27.6	6.1	[1]
		34	37	24.4		
Ni-15Cr-8Fe		13	24	26.5	14.7	
		34	36	23.7		
Ni-26Cr-8Fe		13	34	37.5	26.5	
		34	55	36.2		
Ni-35Cr-8Fe		13	60	66.2	34.8	
		34	99	65.2		
Hastelloy C-22 (heat S08)	573	138	110	30.3	21.8	[23]
Hastelloy X	723	30	60 cm^3/100g	38.5	21.7	[5]

† calculated assuming density of 8.2 g/cm^3 for all alloys; actual density of some alloys is greater

Table 3.1.1.1. Tensile properties of solid-solution Ni-Cr alloys at room temperature: measured in air with internal hydrogen (thermal precharging in gaseous hydrogen), or measured in high-pressure gaseous helium and hydrogen; values in parenthesis are estimated.

Material	Thermal precharging	Test environment	Strain rate (s^{-1})	S_y (MPa)	S_u (MPa)	El_u (%)	El_t (%)	RA (%)	Ref.
Inconel 600	None	Air	0.67 x10^{-3}	280	710	—	—	75	[21]
	(1)	Air		(280)	(710)	—	—	66	
Inconel 625	None	Air	0.67 x10^{-3}	330	805	—	—	43	[21]
	(1)	Air		(330)	(805)	—	—	28	
Inconel 625 (heat H73a)	None	34.5 MPa He	0.17 x10^{-3}	579	1002	—	47	62	[20, 27]
	None	34.5 MPa H_2		694	975	—	23	30	
Inconel 625 (heat W73)	None	Air	—	648	993	—	50	54	[28]
	None	34.5 MPa He		634	993	—	55	50	
	None	34.5 MPa H_2		600	993	—	20	18	
Inconel 690 (heat S98a)	None	Air	0.4 x10^{-3}	289	668	46	56	70	[22]
	(2)	Air		310	627	41	48	43	
	(3)	Air		310	550	27	31	40	
Inconel 690 (heat S98b)	None	Air	0.4 x10^{-3}	282	668	45	52	67	[22]
	(2)	Air		282	550	22	25	32	
	(3)	Air		296	482	11	17	31	
Hastelloy C-22 (heat S08)	None	Air	2 x10^{-3}	383	810	58	89	72	[23]
	(4)	Air		426	793	52	56	41	
Hastelloy X (heat H73c)	None	34.5 MPa He	0.17 x10^{-3}	321	723	—	54	63	[20, 27]
	None	34.5 MPa H_2		340	727	—	53	63	

(1) 24 MPa gaseous hydrogen, 475K, 410 hours
(2) 13 MPa gaseous hydrogen, 558K, 1000 hours; 38 wppm hydrogen
(3) 34 MPa gaseous hydrogen, 558K, 1000 hours; 60 wppm hydrogen
(4) 138 MPa gaseous hydrogen, 573K, 820 hours; 110 wppm hydrogen

Table 3.1.1.2. Tensile properties of solid-solution Ni-Cr alloys at both cryogenic and elevated temperature in gaseous hydrogen and helium at pressure of 34.5 MPa.

Material	Thermal precharging	Test environment	Strain rate (s^{-1})	S_y (MPa)	S_u (MPa)	El_u (%)	El_t (%)	RA (%)	Ref.
Inconel 625 (heat W73)	None	He – 144 K	—	710	1130	—	43	52	[20, 27]
	None	H_2 – 144 K		696	1120	—	43	48	
Inconel 625 (heat H73a)	None	He – 951 K	0.17 x10^{-3}	507	819	—	61	68	[28]
	None	H_2 – 951 K		517	850	—	55	60	
Hastelloy X (heat H73c)	None	He – 951 K	0.17 x10^{-3}	235	550	—	53	58	[28]
	None	H_2 – 951 K		234	555	—	51	54	

Table 3.1.1.3. Tensile properties of Ni–Cr–Fe alloys thermally precharged in gaseous hydrogen and tested in air at room.

Material	Thermal precharging	Test environment	Strain rate (s^{-1})	S_y (MPa)	S_u (MPa)	El_u (%)	El_t (%)	RA (%)	Ref.
Ni–6Cr–8Fe	None	Air	0.4 x10^{-3}	207	462	—	35	45	[1]
	(1)	Air		200	420	—	31	47	
	(2)	Air		220	468	—	31	42	
Ni–15Cr–8Fe	None	Air	0.4 x10^{-3}	282	586	—	49	52	[1]
	(1)	Air		230	510	—	43	48	
	(2)	Air		255	565	—	42	45	
Ni–26Cr–8Fe	None	Air	0.4 x10^{-3}	289	593	—	53	57	[1]
	(1)	Air		255	410	—	22	31	
	(2)	Air		282	427	—	13.5	20	
Ni–35Cr–8Fe	None	Air	0.4 x10^{-3}	261	606	—	55	65	[1]
	(1)	Air		275	454	—	25	36	
	(2)	Air		300	475	—	18	27	

(1) 13 MPa gaseous hydrogen, 558K, 1000 hours
(2) 34 MPa gaseous hydrogen, 558K, 1000 hours

Table 3.1.2.1. Notched tensile properties of solid-solution Ni-Cr alloys at room temperature in high-pressure gaseous helium and hydrogen.

Material	Specimen	Thermal precharging	Test environment	Displ. rate (mm/s)	S_y † (MPa)	σ_s (MPa)	RA (%)	Ref.
Inconel 625 (heat H73a)	(a)	None	34.5 MPa He	2.1×10^{-3}	579	1252	15	[20, 27]
		None	34.5 MPa H_2		694	1227	6.9	
Inconel 625 (heat W73)	(b)	None	34.5 MPa He	0.4×10^{-3}	634	1430	9.4	[28]
		None	34.5 MPa H_2		600	1090	4.6	
Hastelloy X (heat H73c)	(a)	None	34.5 MPa He	2.1×10^{-3}	321	1005	18	[20, 27]
		None	34.5 MPa H_2		340	874	14	

† yield strength of smooth tensile bar

(a) V-notched specimen: 60˚ included angle; minimum diameter = 8 mm (0.315 inch); maximum diameter = 12.7 mm (0.5 inch); notch root radius = 0.051 mm (0.002 inch). Stress concentration factor (K_t) = 8.0.

(b) V-notched specimen: 60˚ included angle; minimum diameter = 3.81 mm (0.15 inch); maximum diameter = 7.77 mm (0.306 inch); notch root radius = 0.024 mm (0.00095 inch). Stress concentration factor (K_t) = 8.4.

Table 3.1.2.2. Notched tensile properties of solid-solution Ni-Cr alloys at both cryogenic and elevated temperature in gaseous hydrogen and helium at pressure of 34.5 MPa.

Material	Specimen	Thermal precharging	Test environment	Displ. rate (mm/s)	S_y † (MPa)	σ_s (MPa)	RA (%)	Ref.
Inconel 625 (heat W73)	(b)	None	He – 144 K	0.4×10^{-3}	710	1460	8.1	[28]
		None	H_2 – 144 K		696	1520	6.9	
Inconel 625 (heat H73a)	(a)	None	He – 951 K	2.1×10^{-3}	507	985	16	[20, 27]
		None	H_2 – 951 K		517	1014	16	
Hastelloy X (heat H73c)	(a)	None	He – 951 K	2.1×10^{-3}	235	625	18	[20, 27]
		None	H_2 – 951 K		234	621	19	

† yield strength of smooth tensile bar

(a) V-notched specimen: 60˚ included angle; minimum diameter = 8 mm (0.315 inch); maximum diameter = 12.7 mm (0.5 inch); notch root radius = 0.051 mm (0.002 inch). Stress concentration factor (K_t) = 8.0.

(b) V-notched specimen: 60˚ included angle; minimum diameter = 3.81 mm (0.15 inch); maximum diameter = 7.77 mm (0.306 inch); notch root radius = 0.024 mm (0.00095 inch). Stress concentration factor (K_t) = 8.4.

Table 3.2.1. Fracture toughness of solid-solution Ni-Cr alloys at room temperature: measured in air with internal hydrogen (thermal precharging in gaseous hydrogen), or measured in high-pressure gaseous helium and hydrogen.

Material	Test method	Thermal precharging	Test environment	S_y (MPa)	K_Q (MPa $m^{1/2}$)	Ref.
Inconel 625 (heat H73b)	LEFM, CT (ASTM E399-72)	None	34.5 MPa He	—	59 † (RL §) 63 † (LR §)	[20]
		None	34.5 MPa H_2	—	66 † (RL §) 60 † (LR §)	
Inconel 625 (heat W73)	LEFM, CT (ASTM E399-72)	None None	34.5 MPa He 34.5 MPa H_2	634 600	84 67	[28]
Inconel 690 (heat S98a)	J-integral, CT (ASTM E813)	None (1)	Air Air	289	330 ‡ 218 ‡†	[22]
Inconel 690 (heat S98b)	J-integral (ASTM E813)	None (1)	Air Air	282	330 ‡ 218 ‡†	[22]

LEFM = linear elastic fracture mechanics; CT = compact tensile

† valid K_{IC} or J_{IC} value according to testing standard

‡ calculated from J; assuming E = 207 GPa, $\nu = 0.3$ and $K = \left[JE/\left(1-\nu^2\right)\right]^{1/2}$; initial loading rate of 1 MPa $m^{1/2}$ per minute

§ RL and LR refer to orientations as defined in ASTM standards for fracture testing, but are inferred from author description of longitudinal and transverse respectively

(1) 13 MPa gaseous hydrogen, 558K, 1000 hours; 38 wppm hydrogen

Table 3.2.2. Fracture toughness of Inconel 625 at temperature of 144 K in gaseous hydrogen and helium at pressure of 34.5 MPa.

Material	Test method	Thermal precharging	Test environment	S_y (MPa)	K_Q (MPa $m^{1/2}$)	Ref.
Inconel 625 (heat W73)	LEFM, CT (ASTM E399-72)	None None	He – 144 K H_2 – 144 K	710 696	110 108	[28]

LEFM = linear elastic fracture mechanics; CT = compact tensile

Table 4.3.1. Tensile properties of welded Inconel 625 at room temperature in high-pressure hydrogen and helium gas.

Material	Thermal precharging	Test environment	Strain rate (s^{-1})	S_y (MPa)	S_u (MPa)	El_u (%)	El_t (%)	RA (%)	Ref.
Welded ‡ Inconel 625 (heat H73a)	None	34.5 MPa He	0.17 x10^{-3}	370	736	—	24	38	[20, 27]
	None	34.5 MPa H_2		363	766	—	25	38	

‡ gas tungsten arc weld (GTAW), using AMS 5837 filler material

Table 4.3.2. Notched tensile properties of welded Inconel 625 at room temperature in high-pressure hydrogen and helium gas.

Material	Specimen	Thermal precharging	Test environment	Displ. rate (mm/s)	S_y † (MPa)	σ_s (MPa)	RA (%)	Ref.
Welded ‡ Inconel 625 (heat H73a)	(a)	None	34.5 MPa He	2.1 x 10^{-3}	370	980	14	[20, 27]
		None	34.5 MPa H_2		363	892	12	

‡ gas tungsten arc weld (GTAW), using AMS 5837 filler material
† yield strength of smooth tensile bar
(a) V-notched specimen: 60˚ included angle; minimum diameter = 8 mm (0.315 inch); maximum diameter = 12.7 mm (0.5 inch); notch root radius = 0.051 mm (0.002 inch). Stress concentration factor (K_t) = 8.0.

Table 4.3.3. Fracture toughness of welded Inconel 625 at room temperature.

Material	Test method	Thermal precharging	Test environment	S_y (MPa)	K_Q (MPa $m^{1/2}$)	Ref.
Welded ‡ Inconel 625 (heat H73b)	LEFM, CT (ASTM E399-72)	None	34.5 MPa He	—	57 † (RL §) 55 † (LR §)	[20]
		None	34.5 MPa H_2	—	61 † (RL §) 59 † (LR §)	

LEFM = linear elastic fracture mechanics; CT = compact tensile
‡ gas tungsten arc weld (GTAW), using AMS 5837 filler material
† valid K_{IC} or J_{IC} value according to testing standard
§ RL and LR refer to orientations as defined in ASTM standards for fracture testing, but are inferred from author description of longitudinal and transverse respectively

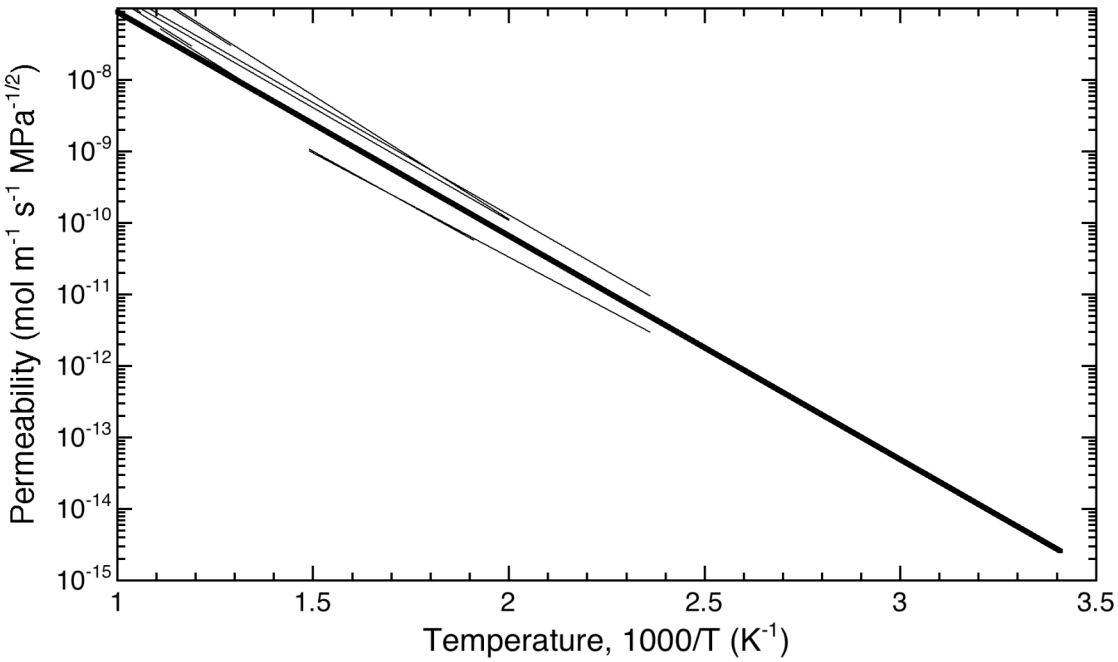

Figure 2.1. Permeability for several solid-solution Ni-Cr alloys from gas permeation experiments. All data corrected to hydrogen. The dark line represents the recommendation for austenitic stainless steels from Ref. [36].

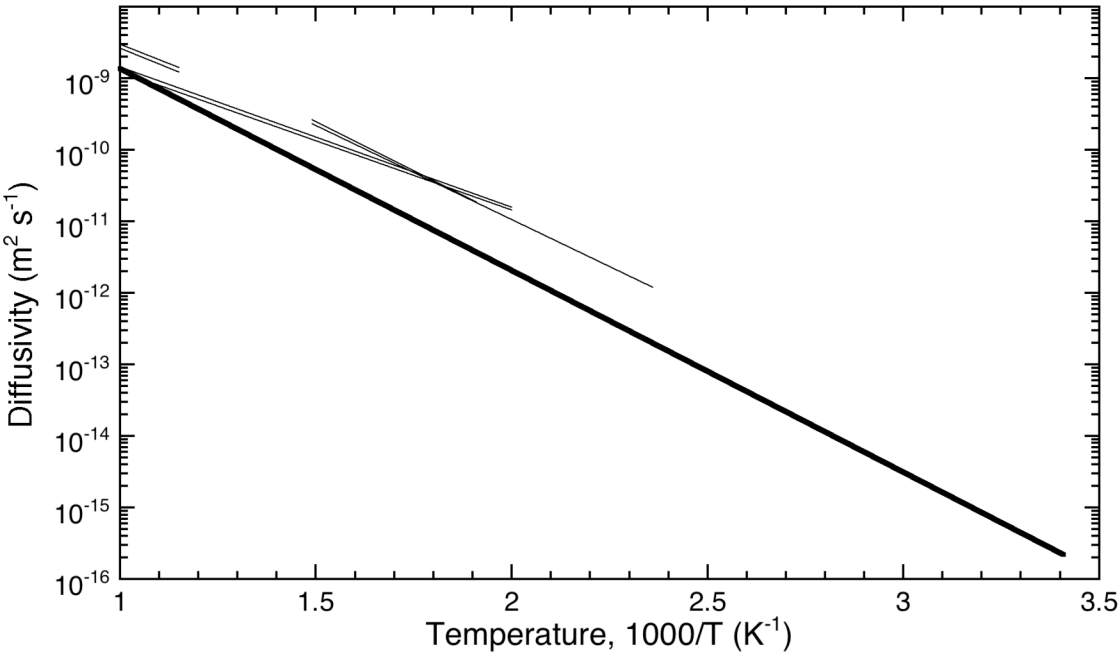

Figure 2.2. Diffusivity of several solid-solution Ni-Cr alloys from gas permeation experiments. All data corrected to hydrogen. The dark line represents the recommendation for austenitic stainless steels from Ref. [36].

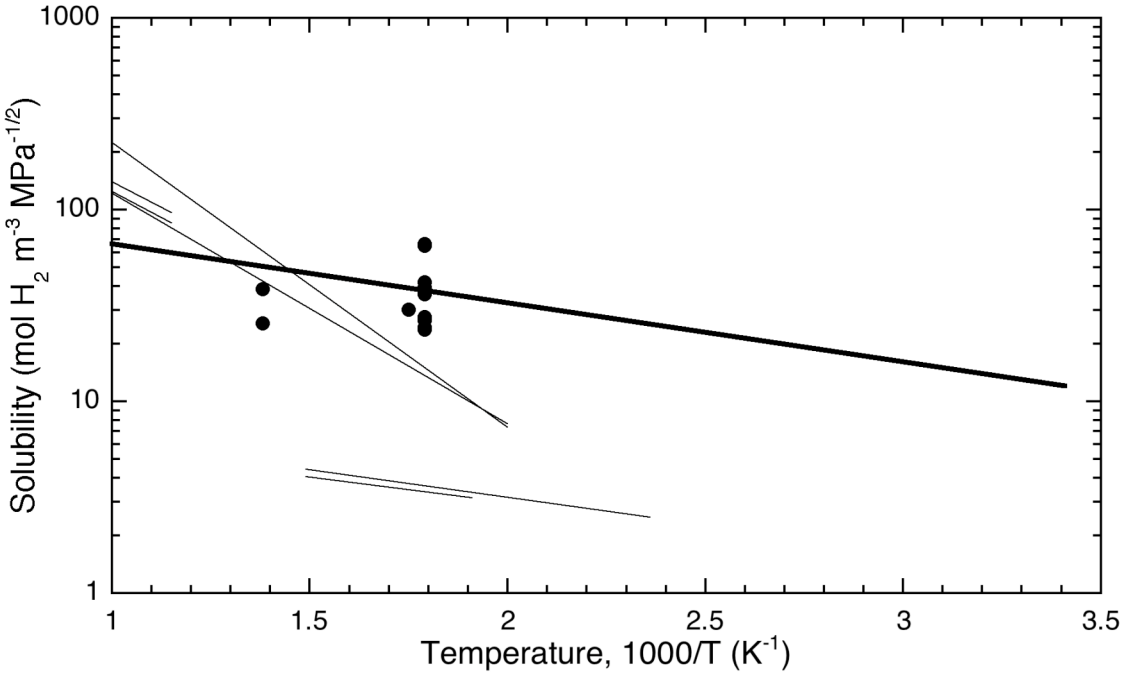

Figure 2.3. Solubility of several solid-solution Ni-Cr alloys from gas permeation experiments. All data corrected to hydrogen. The dark line represents the recommendation for austenitic stainless steels from Ref. [36]. The data points are values determined from equilibrium concentration measurements (i.e., thermal precharging) reported in Table 2.2.

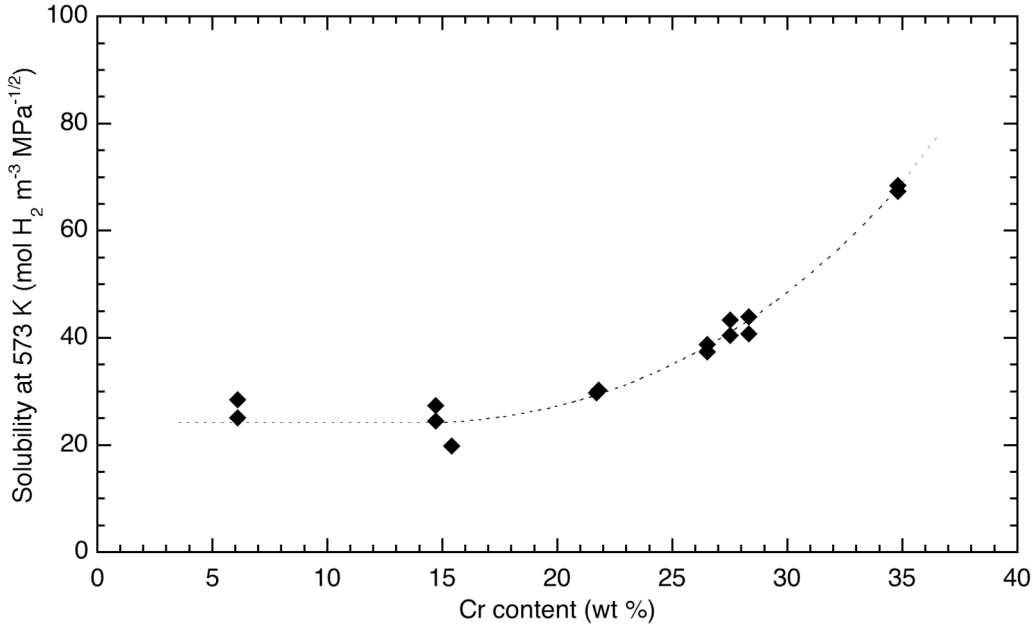

Figure 2.4. Calculated solubility from equilibrium concentration measurements plotted as a function of chromium content. Reported hydrogen concentrations are given in Table 2.2. The solubility is calculated and then corrected to temperature of 573 K assuming the temperature dependence of austenitic stainless steel (E_S = 5.9 kJ/mol) and density of 8.2 g/cm^3.

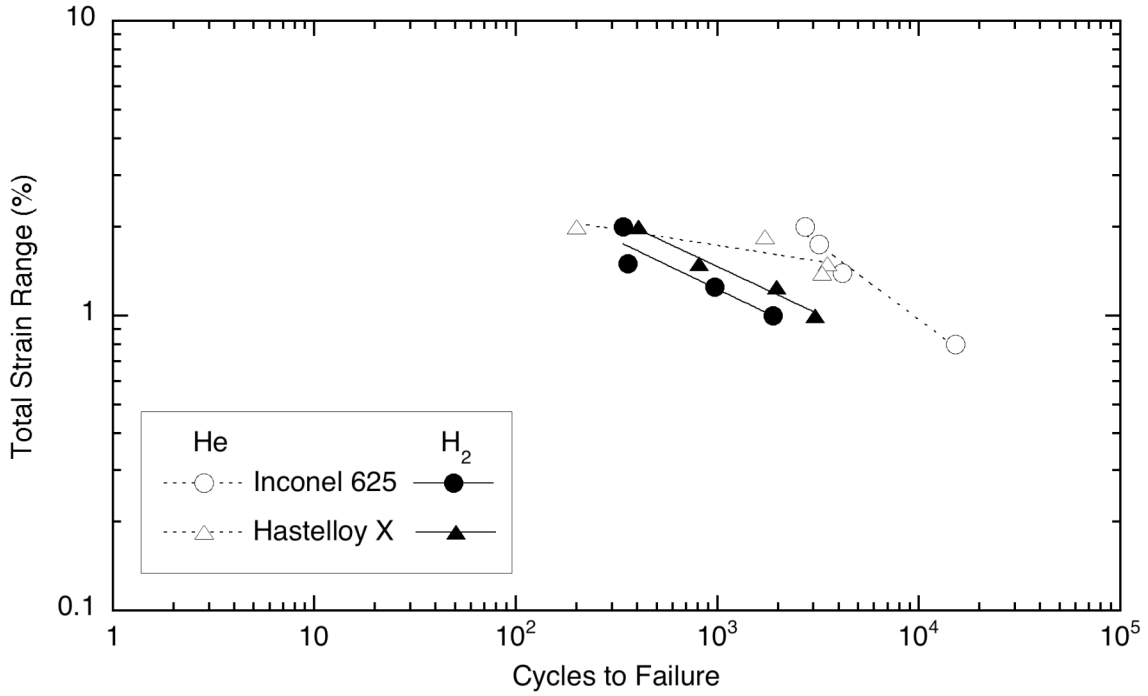

Figure 3.3.1. Low-cycle fatigue in gaseous helium and hydrogen at pressure of 34.5 MPa [20, 27].